

Josephson Effects in Frequency-Domain Multiplexed TES Microcalorimeters and Bolometers

Gottardi, L.; Smith, S. J.; Kozorezov, A.; Akamatsu, H.; Bruijn, M. P.; Chervenak, J. A.; Gao, J. R.; Jackson, B. D.; Ridder, M.; More Authors

DOI

[10.1007/s10909-018-2006-0](https://doi.org/10.1007/s10909-018-2006-0)

Publication date

2018

Document Version

Accepted author manuscript

Published in

Journal of Low Temperature Physics

Citation (APA)

Gottardi, L., Smith, S. J., Kozorezov, A., Akamatsu, H., Bruijn, M. P., Chervenak, J. A., Gao, J. R., Jackson, B. D., Ridder, M., & More Authors (2018). Josephson Effects in Frequency-Domain Multiplexed TES Microcalorimeters and Bolometers. *Journal of Low Temperature Physics*, 193(3-4), 209-216. <https://doi.org/10.1007/s10909-018-2006-0>

Important note

To cite this publication, please use the final published version (if applicable).
Please check the document version above.

Copyright


Other than for strictly personal use, it is not permitted to download, forward or distribute the text or part of it, without the consent of the author(s) and/or copyright holder(s), unless the work is under an open content license such as Creative Commons.

Takedown policy

Please contact us and provide details if you believe this document breaches copyrights.
We will remove access to the work immediately and investigate your claim.



Josephson Effects in Frequency-Domain Multiplexed TES Microcalorimeters and Bolometers

L. Gottardi¹  · S. J. Smith^{2,3} · A. Kozorezov⁴ · H. Akamatsu¹ · J. van der Kuur⁵ · S. R. Bandler⁶ · M. P. Bruijn¹ · J. A. Chervenak⁶ · J. R. Gao^{1,7} · R. H. den Hartog¹ · B. D. Jackson⁵ · P. Khosropanah¹ · A. Miniussi⁸ · K. Nagayoshi¹ · M. Ridder¹ · J. Sadleir⁶ · K. Sakai⁹ · N. Wakeham⁸

Received: 2 November 2017 / Accepted: 18 June 2018
© Springer Science+Business Media, LLC, part of Springer Nature 2018

Abstract

Frequency-division multiplexing is the baseline read-out system for large arrays of superconducting transition-edge sensors (TES's) under development for the X-ray and infrared instruments like X-IFU (Athena) and SAFARI, respectively. In this multiplexing scheme, the sensors are ac-biased at different frequencies from 1 to 5 MHz and operate as amplitude modulators. Weak superconductivity is responsible for the complex TES resistive transition, experimentally explored in great detail so far, both with dc- and ac-biased read-out schemes. In this paper, we will review the current status of our understanding of the physics of the TES's and their interaction with the ac bias circuit. In particular, we will compare the behaviour of the TES nonlinear impedance, across the superconducting transition, for several detector families, namely: high-normal-resistance TiAu TES bolometers, low-normal-resistance MoAu TES microcalorimeters and high-normal-resistance TiAu TES microcalorimeters.

Keywords Josephson effect · Frequency-domain multiplexing · Transition-edge sensors

1 Introduction

The XIFU [1] and the SAFARI [2] instruments on the future X-ray and infrared space missions Athena and SPICA, respectively, will use the MHz frequency-domain multiplexing (FDM) technology for the read-out of large arrays of superconducting transition-edge sensors (TESs). In the MHz-FDM scheme, the TESs are ac-biased in

✉ L. Gottardi
l.gottardi@sron.nl
<http://www.sron.nl>

Extended author information available on the last page of the article

the frequency range from 1 to 5 MHz and they work as amplitude modulators. The TES detector physics and its interaction with the read-out circuit are not completely understood. The TES behaviour under dc and ac bias is strongly affected by proximity effects caused by the connection to the higher T_c superconducting Nb leads and by the normal metal structures introduced to suppress the excess noise [3–8]. The TES behaves typically as an SS'S or SNS junction, and the Josephson effects are regularly observed both in the response to the perpendicular magnetic field and, under ac bias, in the changes of the TES reactance across the superconducting transition. Furthermore, in ac-biased low-ohmic TES microcalorimeters, the Josephson effects are masked by another frequency-dependent dissipation mechanism, on which we have reported before [9] and which is related to the generation of eddy currents in the normal metal structures surrounding the TES. This effect has been systematically studied and the major sources of ac loss identified [10]. In the framework of the single pixel optimization for FDM, it turns out to be useful to compare the performance of detectors with different physical parameters like the normal resistance R_N , the saturation power P , the TES size, the TES-absorber coupling topology, and the geometry of the normal metal structures on the TES. This study is an ongoing process [9], and in this paper, we will focus on the scaling of the Josephson effect with the resistance and the saturation power of low-ohmic MoAu TES microcalorimeters developed at NASA-Goddard and high-ohmic TiAu TES's bolometers and microcalorimeters. For the high-ohmic TiAu SRON TES bolometers and one sample of the low-ohmic MoAu NASA-Goddard microcalorimeter, we also show the dependency on the bias frequency. We discuss only the results obtained with bare TES's without the normal-metal noise-mitigating stripes.

2 RSJ Model for TES Microcalorimeters Under AC Bias

We review here the theoretical framework currently adopted to explain the experimental observations made so far when a TES works as an amplitude modulator of a MHz signal. The electrical circuit for a single pixel in a FDM system can be simplified as shown in Fig. 1. Here, we neglect the effect of the superconducting transformer normally used with low-ohmic devices to match the impedance of low-ohmic devices to the LC filter and the Superconducting QUantum Interference Devices (SQUIDs). Therefore, for the low-ohmic MoAu NASA-Goddard detector the values of the filter inductance L , the SQUID impedance, the bias voltage and the SQUID current noise are transformed to the values that would be seen at the input of the TES. Typically, a transformer ratio between 4 and 6 is used.

We consider the TES as a superconducting film S' connected to the two superconducting Nb leads S and forming in this way a small, 1-dimensional, $SS'S$ proximity induced weak-link. Generally, to model the TES, one has to solve the dc and ac Josephson equations simultaneously with the power balance relation [11]. The total current $I(t)$ flowing in the TES is considered to be the sum of two components, a pair (or Josephson) current $I_J = I_0 \sin \varphi$ and a quasi-particle current $I_{qp} = V(t)/R$, where φ is the gauge-invariant phase difference between the wave functions of the two superconductors S , I_0 is the TES critical current, $V(t) = V_0 \cos(\omega_0 t)$ is the oscillating voltage across the TES and $R(\varphi)$ is a phase-dependent resistance. The RSJ model

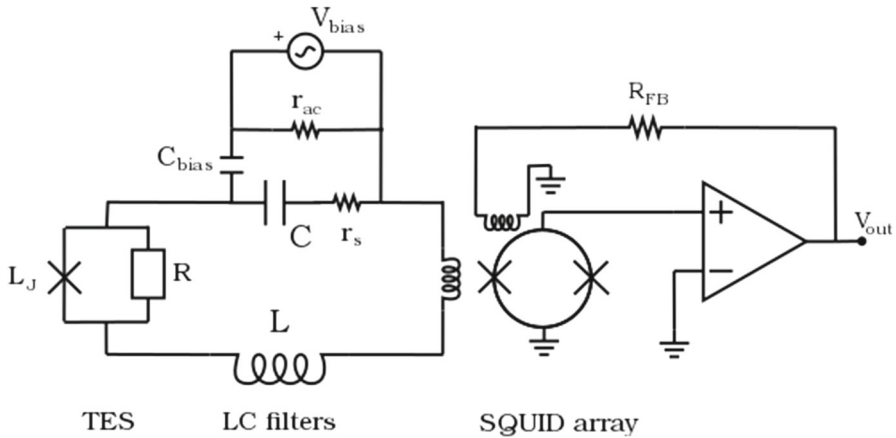


Fig. 1 Simplified electrical circuit for a single pixel ac bias read-out of a TES-based bolometer or microcalorimeter

assumes this resistance to be constant and equal to the weak-link normal resistance R_N . Despite this simplification of the problem, the RSJ model has been widely used to explain the major effects observed in many types of weak-links and Josephson junctions [12], including the TES-based detectors biased at MHz frequencies [8,9]. In the case of an ac voltage-biased TES, the gauge-invariant phase φ oscillates at the bias frequency ω_0 , is $\pi/2$ -out-phase with the voltage and its peak value is proportional to V_0/ω_0 . An analytical solution can be found for the stationary nonlinear response of an ac-biased TES [8,11].

In an equivalent electrical circuit, the TES can be represented by a resistance in parallel with the nonlinear Josephson inductance L_J , whose inverse is given by $L_J^{-1} = \frac{2\pi}{\Phi_0} I_0 \cos \varphi$, where $\Phi_0 = 2.067 \cdot 10^{-15}$ Wb is the magnetic flux quantum and we assume a sinusoidal current-phase relation for the TES. The inverse inductance describes the energy exchange rate of the junction with the coupled electrical circuit. The Josephson inductance is a non-dissipative element in the FDM circuit and can be derived from the quadrature component of the measured I–V characteristics in the FDM read-out. The Josephson inductance depends on the physical properties of the weak-link and the bias conditions. Along with the resistive transition, it provides information for the optimization of the TES read-out in the frequency domain. In the following section, we will study the dependency of the Josephson inductance over the transition of TES-based microcalorimeters and bolometers.

3 Experimental Results

We report here the results obtained with detectors developed both at NASA-Goddard and SRON, all based on bare TES's without the noise-mitigating normal metal structure. We will consider: microcalorimeters made of MoAu bi-layer TES's, with sizes of $50 \times 50 \mu\text{m}$ and $100 \times 100 \mu\text{m}$, from a mixed 8×8 array fabricated at NASA-Goddard [10,13]; a $140 \times 160 \mu\text{m}$ microcalorimeter with a TiAu TES, from a 5×5

Table 1 Parameters of the TES detectors from SRON and NASA-Goddard

TES	Bi-layer	Size ($\mu\text{m} \times \mu\text{m}$)	R_N ($\text{m}\Omega$)	Power (pW)	Comments
SRON bolometers	TiAu	50×50	100	$\sim 3 \times 10^{-3}$	Figs. 2 and 3a, b
GSFC μ -cal*	MoAu	50×50	7–8	2–4	Figs. 2 and 3c, d
GSFC μ -cal	MoAu	100×100	9	10	Figs. 2 and 3e
SRON μ -cal	TiAu	140×160	220	8–10	Figs. 2 and 3f

* These pixels were characterized at NASA-Goddard in an ADR cooler hosting SRON/VTT FDM read-out cold and warm electronics

array fabricated at SRON; and $50 \times 50 \mu\text{m}$ SRON TES bolometers [14]. The main properties of these detectors are given in Table 1. The measurements were done with the FDM systems developed at SRON [9,10,14,15].

In Fig. 2, we show the Josephson inductance L_J , normalized to the TES resistance R , as a function of R/R_N . The data are derived from the TES I - V characteristics using the in-phase and quadrature information. The local minima and local maxima indicated on each plot are the points at which the inverse of the Josephson inductance has its maximum, i.e. $\cos \varphi = \pm 1$. The local minima correspond to values of the weak-link gauge-invariant phase $\varphi = n\pi$, with $n = 0, 2, 4, \dots$, and the local maxima to $\varphi = (n + 1)\pi$.

We observe that when the detectors are biased at higher frequencies, the absolute value of $\omega_0 L_J/R$, at the local minima and maxima and for a comparable R/R_N value, decreases with increasing bias frequency. This is best seen by looking at the two pairs of plots (a,b) and (c,d) of Fig. 2. Moreover, detectors with larger power show higher values of $\omega_0 L_J/R$: in the same figure, the plots are sorted such that the detector power increases with the letters order, i.e. (a) and (b) have the lowest power and (f) the highest. Finally, lower values of $\omega_0 L_J/R$ are observed in low-ohmic devices. As a result of this, low-ohmic, low-power detectors biased at high frequency generally show, under ac bias, stronger Josephson effects, which can be quantified by looking at the ratio I_Q/I_I between the detector quadrature and in-phase current, as shown in Fig. 3.

The SRON low-power TES bolometers (Fig. 3 (a), (b)) show the higher I_Q/I_I ratio, reaching values of about 25% when biased for example at $R/R_N = 0.2$, even when they are measured at lower bias frequency with respect for example to the microcalorimeters. On the contrary, the Josephson current measured in SRON TES microcalorimeters (Fig. 3f), with high power P and high normal resistance R_N , is very small with $I_Q/I_I < 5\%$ over the whole TES transition. The ratio I_Q/I_I is typically around 10% for the GSFC calorimeters (Fig. 3c–e) at the optimal bias point around $R/R_N = 0.2$.

The strength of the Josephson effects observed in TES devices scales with the value of the gauge-invariant superconducting phase difference across the weak-link defined by the second Josephson equation $\varphi = \sqrt{PR}/\omega_0$, written here in terms of detector power P and resistance R . This follows naturally from the RSJ model: the higher the phase difference and the lower the Josephson effects. High saturation power, high normal resistance and low bias frequency read-out is one way to minimize the weak-

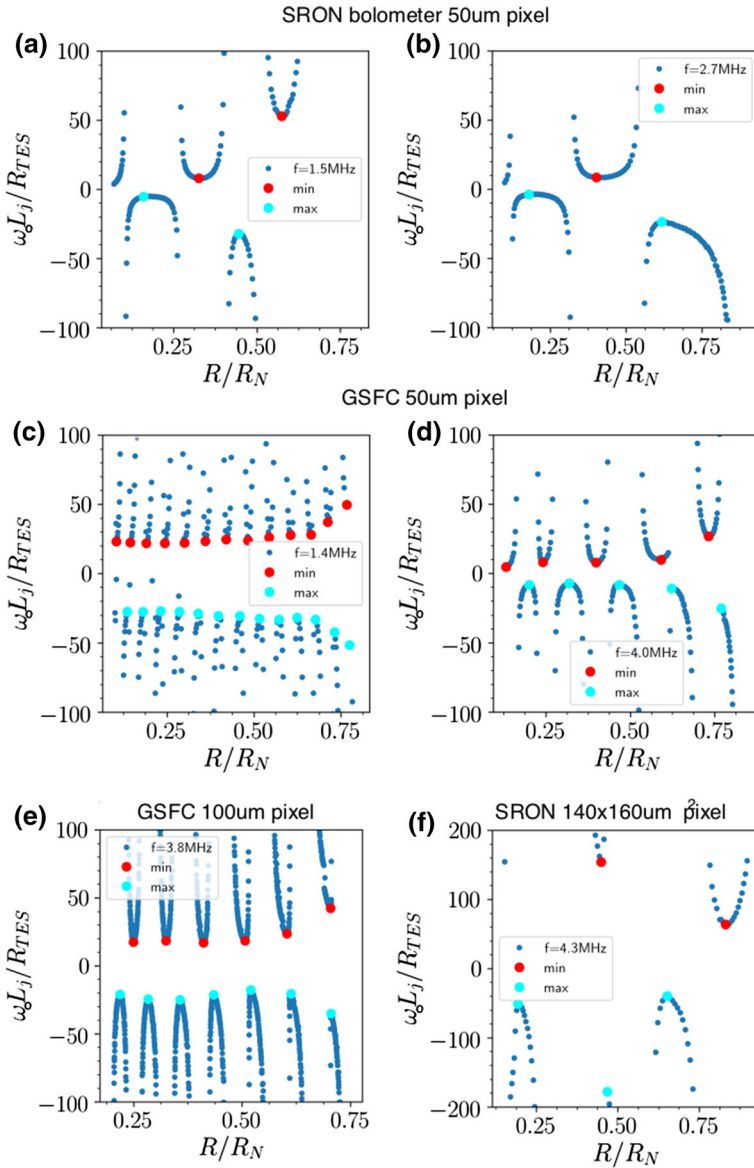


Fig. 2 Normalized Josephson inductance $\omega_0 L_j / R$ as a function of R/R_N for the detectors under study. **a, b** SRON TiAu TES bolometers; **c, d** GSFC MoAu, 50µm TES microcalorimeters; **e** GSFC MoAu, 100µm TES microcalorimeters; **f** SRON TiAu, 140µm × 160µm TES microcalorimeters. Note that the vertical scale is a factor of two higher than other plots. The local minima (red dots) correspond to values of the weak-link gauge-invariant phase $\varphi = n\pi$, with $n = 0, 2, 4, \dots$, and the local maxima (cyan dots) to $\varphi = (n + 1)\pi$. (Color figure online)

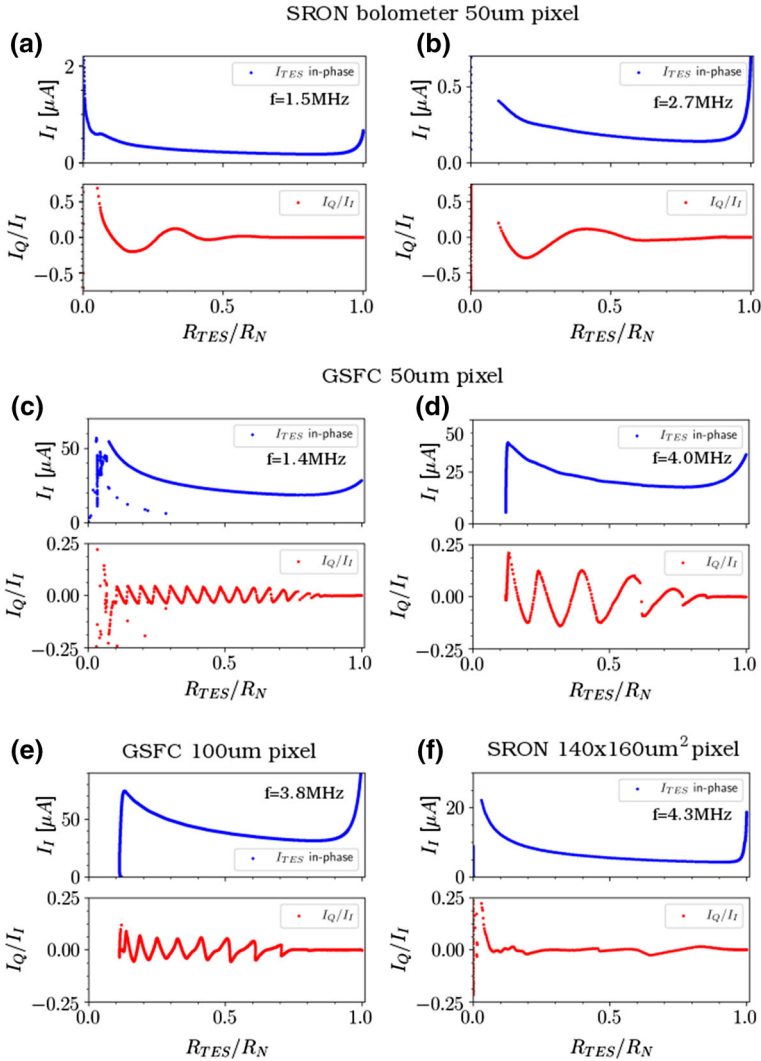


Fig. 3 TES current in-phase I_I (upper graph) and the ratio between the quadrature and in-phase current I_Q/I_I (lower graph), as a function of R/R_N for the detectors under study. **a, b** SRON TiAu TES bolometers; **c, d** GSFC MoAu, 50 μm TES microcalorimeters; **e** GSFC MoAu, 100 μm TES microcalorimeters; **f** SRON TiAu, 140 $\mu\text{m} \times 160\mu\text{m}$ TES microcalorimeters. (Color figure online)

link effects in TES's. The power and the bias frequency is typically constrained by the scientific application and by the engineering requirements. The only parameter left free for the optimization is the TES normal resistance. This is at least true in the case of an ideal weak-link. The TES size and the normal metal structure used to suppress the excess noise in microcalorimeters contribute as well in shaping the TES resistive transition [4,5]. The physical processes in the TES are then more complicated than the ideal case considered here [9,16] and a better understanding of those processes is essential to further optimize the detectors both in the dc and ac bias configuration.

4 Conclusions


We have reported on the behaviour of the TES nonlinear impedance, along the superconducting transition, for several detector families with different physical parameters. The results presented here are only a small sample of the data analysed so far. Nevertheless, they are representative of the behaviour typically observed in TES's read-out in FDM from 1 to 5 MHz. Detectors with high saturation power and high normal resistance, biased at low frequency, show generally small or negligible Josephson current under ac bias. The Josephson effects are non-dissipative. They do not add noise to the detector, but they introduce undesired, bias dependent, nonlinearities, which limit the optimal bias range. To simplify the read-out of large TES array, these effects should be minimized. We believe that a way to mitigate the weak-link behaviour in ac-biased detectors is to increase the normal resistance of the TES's for the same power.

Acknowledgements H.A acknowledges the support of NWO via a Veni grant. SRON is supported financially by NWO, the Netherlands Organization for Scientific Research.

References

1. D. Barret, Proc. SPIE, Space Telescopes and Instrumentation 2014: Ultraviolet to Gamma Ray, **9905**, 99052F,(2016)
2. P. Roelfsema, Proc. SPIE **9143**, 9143–9154 (2014)
3. J.E. Sadleir, S.J. Smith, S.R. Bandler, J.A. Chervenak, J.R. Clem, Phys. Rev. Lett. **104**, 047003 (2010)
4. J.E. Sadleir, S.J. Smith, S.R. Bandler, J.A. Chervenak, J.R. Clem, Phys. Rev. B **84**, 184502 (2011)
5. S.J. Smith et al., J. Appl. Phys. **114**, 074513 (2013)
6. J.N. Ullom, D.A. Bennett, Supercond. Sci. Technol. **28**, 084003 (2015)
7. L. Gottardi et al., J. Low Temp. Phys. **167**, 214 (2012)
8. L. Gottardi et al., Appl. Phys. Lett. **105**, 162605 (2014)
9. L. Gottardi et al., IEEE Trans. Appl. Supercond. **27**(4), 1–4 (2017)
10. K. Sakai et al., J. Low Temp. Phys. (2018). <https://doi.org/10.1007/s10909-018-2002-4>
11. A. Kozorezov et al., Appl. Phys. Lett. **99**, 063503 (2011)
12. K. Likharev, Rev. Mod. Phys. **51**, 101 (1979)
13. A. Miniussi et al., J. Low Temp. Phys. (2018). <https://doi.org/10.1007/s10909-018-1974-4>
14. P. Khosropanah et al., Proc. SPIE **9144**, 9914-9914-5 (2016)
15. H. Akamatsu et al., J. Low Temp. Phys. **176**(3–4), 591–596 (2014)
16. N. Wakeham et al., J. Low Temp. Phys. (2018). <https://doi.org/10.1007/s10909-018-1898-z>

Affiliations

L. Gottardi¹  · S. J. Smith^{2,3} · A. Kozorezov⁴ · H. Akamatsu¹ · J. van der Kuur⁵ · S. R. Bandler⁶ · M. P. Bruijn¹ · J. A. Chervenak⁶ · J. R. Gao^{1,7} · R. H. den Hartog¹ · B. D. Jackson⁵ · P. Khosropanah¹ · A. Miniussi⁸ · K. Nagayoshi¹ · M. Ridder¹ · J. Sadleir⁶ · K. Sakai⁹ · N. Wakeham⁸

¹ SRON National Institute for Space Research, Sorbonnelaan 2, 3584 CA Utrecht, The Netherlands

² NASA Goddard Space Flight Center, Greenbelt, MD 20771, USA

- ³ CRESST and University of Maryland, Baltimore County, MD 21250, USA
- ⁴ Department of Physics, Lancaster University, LA1 4 Lancaster, UK
- ⁵ SRON Netherlands Institute for Space Research, Landleven 12, 9747 AD Groningen, The Netherlands
- ⁶ NASA Goddard Space Flight Center, Greenbelt, MD 20771, USA
- ⁷ Kavli Institute of NanoScience, Faculty of Applied Sciences, Delft University of Technology, Lorentzweg 1, 2628 CJ Delft, The Netherlands
- ⁸ NASA Postdoctoral Program, Universities Space Research Assoc., Greenbelt, MD 20771, USA
- ⁹ CRESST II - UMBC, 1000 Hilltop Circle, Baltimore, MD 21250, USA